



The impact of urbanization on air stagnation: Shenzhen as case study

Zhiqiang Li ^{a,1}, Yulun Zhou ^{b,g,1}, Bingcheng Wan ^c, Qinxin Chen ^d, Bo Huang ^{a,b,*}, Yuanzheng Cui ^e, Hopun Chung ^f

^a Institute of Space and Earth Information Science, The Chinese University of Hong Kong, 999077, Hong Kong, China

^b Department of Geography and Resource Management, The Chinese University of Hong Kong, 999077, Hong Kong, China

^c Glarun Technology Co., Ltd, Nanjing 211100, China

^d School of Statistics, Southwestern University of Finance and Economics, Chengdu 611130, China

^e Institute of Land and Urban-rural Development, Zhejiang University of Finance and Economics, Hangzhou 310018, China

^f Department of Computer Science and Engineering, The Chinese University of Hong Kong, 999077, Hong Kong, China

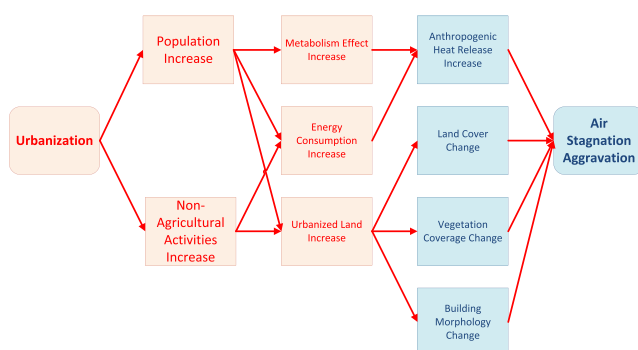
^g Faculty of Geosciences and Environmental Engineering, Southwest Jiaotong University, Chengdu 611756, China



HIGHLIGHTS

- Regulating mechanism of urbanization on air stagnation
- Urban climate modelling
- Urbanization worsened the problem of air stagnation.

GRAPHICAL ABSTRACT



ARTICLE INFO

Article history:

Received 13 August 2018

Received in revised form 18 January 2019

Accepted 19 January 2019

Available online 2 February 2019

Editor: SCOTT SHERIDAN

Keywords:

Urban air pollution

Urban climate change

Land use change

Urban planning

WRF/Noah LSM/SLUCM

China

ABSTRACT

One of the most concerning consequences arising from the dramatic urbanization in cities is air stagnation and the related high concentration of air pollutants. Many studies have investigated the impact of urbanization on air stagnation, but few have systematically evaluated such impact and its spatial-temporal variances at the municipal scale. This study proposed an approach based on high-resolution urban climate simulations for evaluating the impact of urbanization on air stagnation. We took the city of Shenzhen in south-eastern China, a city that grew from a small fishing and farming village to a highly urbanized city in the past thirty years, as a compelling case study. Using the WRF/Noah LSM/SLUCM model, we simulated and evaluated the probability of 6-hourly air stagnation cases (ASCs) in 1979 and 2010 at the spatial resolution of 1-km² to demonstrate the change over a thirty-year period. Comparison results show that urbanization worsened the problem of air stagnation in Shenzhen. The number of 6-hourly ASCs has increased by 21,700 for the entire Shenzhen, and by 11.4 on average for each grid with a 1 km² size. A maximum increase of 458 ASCs in a grid was also observed.

© 2019 Published by Elsevier B.V.

* Corresponding author at: Institute of Space and Earth Information Science, Fok Ying Tung Remote Sensing Science Building, The Chinese University of Hong Kong, Shatin, NT 999077, Hong Kong, China.

E-mail address: bohuang@cuhk.edu.hk (B. Huang).

¹ Zhiqiang Li and Yulun Zhou contributed equally to this work and should be considered co-first authors.

1. Introduction

Urban air pollution has been pervasive in most of the world since the start of industrialization (Mayer, 1999), while far before industrialization, since ancient Roman Empire time, urban dwellers had been bedeviled by the urban air pollution (Borsos et al., 2003; Havlíček and Morcinek, 2016). In recent years, urban air pollution has progressively become a disturbing social problem in many countries, especially in China, where the deterioration of air quality and its menace to public health safety have been widely reported due to its harmfulness to public health (Mar et al., 2004; Delfino et al., 2008; Halonen et al., 2008; Matus et al., 2012; EEA, 2012; Costa et al., 2014). In China, the rapid and massive urbanization in the past three decades seems to have benefited the urban dwellers by increasing their wealth, but it has also brought harm, primarily through polluting the air (Zhou et al., 2004). Both the Chinese people and the government have realized the compelling necessity to prevent air pollution and identify appropriate measures to help reduce air pollution in the future.

Air stagnation is the phenomenon by which air lasts in an area for an extended period, which can dramatically increase local air pollutants' concentration and the related health risks of dwellers (Korshover and Angell, 1982; Wang and Angell, 1999; Jacob and Winner, 2009; Horton and Diffenbaugh, 2012). An air stagnation case (ASC) is defined as a protracted atmospheric episode characterized by poor air ventilation. Existing studies on poor air ventilation mainly used low near-surface wind speed as a meteorological indicator (Yim et al., 2009; Ng et al., 2011; Edussuriya et al., 2014; and Yuan et al., 2014). However, the dispersion of air pollution in urban spaces can be significantly affected by many other meteorological attributes as well. The criteria of identifying ASCs encompass not only wind speed but also a set of other related meteorological conditions, including the scavenging capability of lower atmospheric wind, the dispersing power of upper atmospheric wind, the effect of precipitation on the vertical escape of pollutants, and the temperature inversion effect on the lower atmospheric wind. More frequent air stagnation could result in higher near-surface concentrations of air contaminants such as particulate matter and ozone (Jacob and Winner, 2009). Despite such significance, few studies have directly identified and analyzed ASCs to understand poor urban air ventilation since the identification of ASCs requires carefully-defined criteria and a comprehensive analysis based on multiple fine-grained meteorological attributes. Even fewer studies were conducted on air stagnation at the municipal scale with fine spatial and temporal resolutions.

The impact of urbanization on air pollution is reflected mainly as deteriorated urban ventilation conditions (Yim et al., 2009; Ng et al., 2011; Yuan et al., 2014) and increased air pollutant emissions in cities (World Health Organization, 2006; Sarzynski, 2012). A major cause of the deteriorated urban ventilation conditions is the changes in land surface properties. Existing studies investigated the relationship between the building morphology (one of land surface properties) and urban wind speed. Focusing on the phenomenon of air stagnation, Horton and Diffenbaugh (2012) and Horton et al. (2014) identified the relationship between the frequency of ASCs, urban population density, and metrics of industrialization. Jacobson et al. (2015) also found an urbanization-induced ring of impact that worsened the air stagnation. However, few studies on the impact of urbanization on air stagnation have considered the effects of detailed changes in urban land surface or focused on the rapidly urbanizing Chinese cities. This work aims to fill this gap.

In this paper, we evaluated the impact of urbanization on air stagnation and investigated its underlying mechanism. We conducted comprehensive urban climate simulations and evaluated ASCs in the context of a rapidly urbanized Chinese city, Shenzhen. By comparing the evaluated air stagnation before and after the thirty years' rapid development, we provided evidences for the impact of urbanization on air stagnation. We first proposed an evaluation scheme that

identifies and evaluates ASCs based on urban meteorological attributes having fine spatial-temporal details. The meteorological attributes were simulated using the WRF/Noah LSM/SLUCM model with an improved urban dataset that considers detailed urbanization-induced changes in the land cover, building morphology, vegetation coverage, and anthropogenic heat fluxes.

The remainder of the paper is organized as follows. Section 2 introduces the applied methodology, including the urbanization impact model and the proposed framework for identifying ASCs based on meteorological attributes. Section 3 introduces the setup of the WRF model, WRF primary data processing, and model evaluation. Section 4 presents the analytical results. Section 5 discusses the causal relationship between urbanization and air stagnation and its physical mechanism. Section 6 summarizes the main conclusion of this work.

2. Methodology

2.1. Study area

The fast-urbanizing cities in China are unique cases for studying the environmental impact of urbanization. As an example of such cities, Shenzhen went through an unprecedentedly rapid and massive urbanization during the past thirty years: the city, once was an aggregation of several small fishing villages in 1979, has grown to be one of the largest metropolitans in China and the world. Geographically, Shenzhen is a coastal city with a territory of about 2000 km² located in Pearl River Delta adjoining Hong Kong, characterized by a subtropical marine climate. In the past thirty years, the city had a skyrocketed growth in its population and economy. The population of Shenzhen increased by more than 33 times from 314,100 in 1979 to 10.47 million in 2010. Shenzhen's GDP went up from 196.38 million RMB in 1979 to 1150.55 billion RMB in 2011 with an average annual growth rate of 24.8% (Statistics Bureau of Shenzhen Municipality, 2013). As a bi-product of such rapid and massive urbanization, Shenzhen is now facing severe air pollution problems, posing a significant health threat to its ten million residents (He et al., 2002; Huang et al., 2012).

2.2. The impact of urbanization on urban climate

To lay the foundation of the proposed analyses, we designed an urbanization impact model that projects the urbanization-induced changes to changes in urban climate (Fig. 1). Complicated interactions exist between urbanization and the urban climate. Urbanization directly increases the population and non-agricultural activities. On the one hand, the increased population needs more urbanized lands for sheltering and other urban functions, which significantly increases the anthropogenic heat release due to increased metabolism and energy consumption. On the other hand, increased non-agricultural activities also increase the amount of urbanized land (for example, lands used for industrial production) and energy consumption, which consequently increases the anthropogenic heat release. The increases in the amount of urbanized land come with dramatic changes in land surface properties, such as the land cover, vegetation coverage, and urban morphology. Collectively, the increase in anthropogenic heat release and changes in land surface properties alter urban land surface processes and near-surface atmospheric circulation and eventually changes the urban climate.

2.3. Identification scheme of air stagnation cases

The identifying method for ASCs was first introduced by Korshover and Angell (1982) who produced the annual and monthly maps of ASCs for a specific area of United States (east of 100° W and between 20° N and 50° N) in 1981 based on the Daily Weather Maps of NOAA's National Weather Service. This method, designed on the theoretical

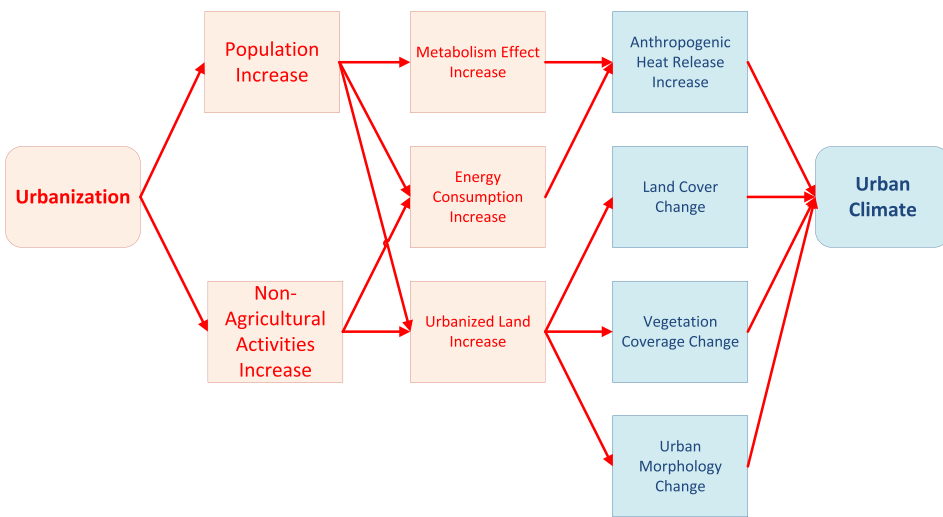


Fig. 1. The impact model of urbanization on urban climate.

foundations laid by other researchers such as Fletcher (1949), Willett (1949), Hewson (1951) and Korshover (1976), included the following four criteria:

- 1) Lower atmospheric horizontal movement: geostrophic surface wind speed lower than 8.0 m/s.
- 2) Upper atmospheric horizontal movement: wind speed at 500 mbar lower than 13.0 m/s.
- 3) Air convective movement: no precipitation.
- 4) Duration: lasting for at least four consecutive days.

In practical calculations, Korshover and Angell (1982) replaced the geostrophic surface wind speed with the surface wind speed as an indicator of lower atmospheric horizontal movement, which became a common practice in succeeding researches (Korshover and Angell, 1987; Wang and Angell, 1999; Leung and Gustafson, 2005; 2014; Huang et al., 2017). In 1999, Wang and Angell (1999) developed a dataset of annual and monthly ASCs from 1948 to 1998 for the entire United States. The Wang and Angell's method also used the surface wind speed as an indicator of lower atmospheric horizontal movement. The major difference between the two methods mentioned above is that the Wang and Angell's method utilized a slightly (10%) higher threshold for lower atmospheric horizontal movement when the temperature inversion occurs below the height of 850 mbar. Succeeding practices of identifying ASCs (Horton and Diffenbaugh, 2012; Horton et al., 2014; Huang et al., 2017) mostly used the Wang and Angell's method with minor changes. Please see Section S1 in Supplementary material for a more detailed review.

Based on the advantages of existing studies, we adopted Wang and Angell's method and applied minor adjustments specific to our study area. First, considering that the geostrophic surface wind is meaningless at low latitudes, we used the surface wind speed as the indicator of the lower atmospheric horizontal movement. Second, we adjusted the threshold on 10-m wind speed when a temperature inversion exists under the height of 850 mbar. Third, the height of the upper atmospheric horizontal movement was set to the height of 850 mbar to match the maximum height used to check the existence of a temperature inversion. We examined each 6-hourly meteorological episode on each 1-km² grid for ASCs satisfying all the following criteria.

- 1) Lower atmospheric horizontal movement: 10-m wind speed lower than 4.0 m/s with the occurrence of a temperature inversion below the height of 850 mbar. 10-m wind speed lower than 4.4 m/s otherwise. The occurrence of a temperature inversion was identified as

episodes when the temperature does not decrease with a 100 m increase in altitude (Wang and Angell, 1999).

- 2) Upper atmospheric horizontal movement: the wind speed at the height of 850 mbar lower than 13.0 m/s without a temperature inversion under the height of 850 mbar.
- 3) Air convective movement: precipitation less than 1 mm.
- 4) Duration: lasting for at least 6 h.

2.4. Experimental design

We respectively simulated urban climate in Shenzhen before and after the thirty years' urbanization. The Case-2010 is a one-year simulation of urban climate in Shenzhen in 2010, while the Case-1979 is a one-year simulation of urban climate in Shenzhen in 1979. Air stagnation cases are identified in both Case-2010 and Case-1979 using the same identification scheme (Section 2.3). The identified ASCs in both cases are compared in terms of the total number, average number per grid, and spatial distributions to provide evidences that supports further explanations of the underlying physical mechanism between urbanization and air stagnation.

3. Technical preparations

3.1. Atmospheric model

We utilized the Weather Research and Forecast (WRF) model as the atmospheric model for simulating urban climate scenarios. The WRF model was developed by National Center for Atmospheric Research (NCAR), went through systematic quality assurance and control, and has been applied extensively in climate diagnostics and predictions (Wang et al., 2015). However, integrating urban land surface processes at municipal scale and fine spatial resolution remains challenging, especially when considering the effects of detailed urban dynamics, such as anthropogenic heat, land cover, vegetation coverage, and urban morphology. Based on existing studies, we improved the model in three ways. First, instead of estimating anthropogenic sensible and latent heat with arbitrary constants, we estimated 2D anthropogenic sensible and latent heat maps and modified the source codes to allow the input into the model. Second, we used a field-surveyed land cover data and remotely-sensed vegetation coverage data to refine the original geographic data provided by the model. Third, we consider the effects of detailed urban morphology on the urban climate by integrating a detailed urban morphology data in the urban canopy model.

3.2. WRF model setup

With these improvements, we set up a telescoping nests' structure including four nested domains centering at 22°39'30" (22.66) N, 114°11'30" (114.19°), the center point of Shenzhen. The spatial resolution of the horizontal grid was set to 1 km in the inner-most domain. Vertically, the same set of 51 vertical eta levels was included in each horizontal domain. There are eight physics components (Cumulus Parameterization, Microphysics, Long-Wave and Short-Wave Radiation, Planetary Boundary Layer, Surface layer, Land Surface Model and Urban Canopy Model) in the model, and different schemes can be chosen for each component (Wang et al., 2015). We selected the New Simplified Arakawa-Schubert scheme as the Cumulus Parameterization component, the WDM5 scheme as the Microphysics component, the RRTMG scheme as the long-wave and short-wave Radiation Component, the Bougeault-Lacarrere scheme as the Planetary Boundary Layer component, the revised MM5 surface layer scheme as the Surface Layer component, the Noah Land Surface Model as the Land Surface Model component, and the Single Layer Urban Canopy Model as the Urban Canopy Model (Table S1). For computational efficiency, each one-year simulation case was divided into a series of subsequent 4-days simulation segments. For more details, please refer to Section S2 in Supplementary material.

3.3. WRF primary data files processing

The Case-1979 and Case-2010 were simulated using the same model setting and lateral boundary conditions but different land surface datasets to reflect urbanization-induced changes in land cover, vegetation coverage, urban morphology, and anthropogenic heat fluxes within Shenzhen. The Case-1979 and Case-2010 respectively used the urban land surface data within Shenzhen in 2010 and 1979. Outside of Shenzhen, both cases used the urban land surface data in 2010 to exclude the effects of urbanization outside of Shenzhen on air stagnation.

The original WRF primary data have limited accuracy and resolution, which may deteriorate the reliability of urban climate simulation results, especially for those with fine spatial-temporal resolutions (Chang et al., 2014). Therefore, we developed high-resolution urban land surface datasets for Shenzhen in both 1979 and 2010, including information about the urban land cover, vegetation coverage, urban morphology, and anthropogenic heat fluxes. The high-resolution land surface data was developed using multiple data sources with sophisticated quality controls including government field surveys and remote sensing imageries. For the land cover data, we first updated the out-of-date land cover map provided by NCAR and then, instead of using one general urban land type, we further classified urban lands into high-, mid- and low-density urban lands based on their respective impervious area fractions so that more detailed variations among urban lands could be simulated. For vegetation coverage, we updated the coarse vegetation coverage maps provided by WRF with high-resolution monthly vegetation coverage maps estimated using cloud-free multi-spectral remote sensing imagery from the Moderate Resolution Imaging Spectroradiometer (MODIS). We also estimated and included an extensive set of urban morphology indicators for high-resolution urban climate simulations, including the urban fraction, area fraction of building plan area fraction, mean building height area weighted, standard deviation of mean building height area weighted, building surface area to building plan area ratio, building height number mean, and frontal area index. Illustrations of the developed high-resolution urban land surface dataset can be found in Section S4 in Supplementary material. Primary data processing packages (*geo_data_refinement* and *wrf_input_refinement*) were also developed to update the variables in WRF primary data with the developed urban land surface dataset.

3.4. Model evaluation

The performance of the atmospheric model used in this study were systematically evaluated by comparing the simulated urban climatological features with the temporal-spatial variations of observed variables such as surface temperature, 2-m air temperature, 10-m wind speed, relative humidity and precipitation using the Perkins Skill Score (PSS, Perkins et al., 2007). The yearly average PSSs for all simulated meteorological attributes were larger than 0.500 while 95% of the monthly PSSs were larger than 0.500, indicating that the model can simulate meteorological details at the resolution of 1-km² appropriately in this study area. For more details of the model evaluation, we refer the readers to Li et al. (n.d.).

4 Results

4.1. Urbanization-induced changes in land cover, vegetation coverage, urban morphology, and anthropogenic heat fluxes

Figs. 2, 3 and 4 show that the urbanization from 1979 to 2010 has induced substantial changes in the land cover, vegetation coverage, urban morphology, and anthropogenic heat fluxes in Shenzhen. For example, the amount of urban land increased dramatically from 5.7 km² in 1979 to around 707.0 km² in 2010, and the amount of vegetation dropped accordingly. We also observed increases in both anthropogenic sensible and latent heat flux (Fig. 3) from close to 0 to about 200 W/m² in some areas over the 30-year period. Such dramatic urbanization-induced changes make the city of Shenzhen a compelling case to study the impact of urbanization on air stagnation.

4.2. Changes in the number of air stagnation cases

The number of ASCs increased remarkably over the thirty years' urbanization in Shenzhen. The maximum increase in the number of ASCs in a grid reached 458, while in the entire Shenzhen, the number of ASCs increased by 21,719 and by 11.4 on average per grid. Fig. 5 shows the difference in the total annual number of ASCs between Case-1979 and Case-2010 (will be referred as the difference of ASCs in the remainder of the paper). Spatially, the number of ASCs increased drastically in some areas, e.g., the Focus-1 area (the lower dashed box in Fig. 5), while it cannot be ignored that in some other areas the number of ASCs decreased, e.g., the Focus-2 area in the northwest of Shenzhen (the upper dashed box in Fig. 5).

5. Discussion

5.1. Cause analyses of the impact of urbanization on air stagnation

Although we have observed an increase in the number of ASCs in Shenzhen over the thirty years' urbanization, the mechanisms linking urbanization and air stagnation are not completely clear. Therefore, we conducted the following cause analyses to find out the mechanism.

First, Fig. 6 represents the differences between two cases in the annual number of ASCs and the ASCs identified only by the surface wind speed (grid meteorological episodes in which 10 m wind speed is equal to or lower than 4.0 m/s together). The pattern of the difference of ASCs (Fig. 6a) is similar to that of the difference in the annual number of 6-hourly grid meteorological episodes in which the 10 m wind speed is equal to or lower than 4.0 m/s (Fig. 6b), which implicates the difference in the annual number of 6-hourly grid meteorological episodes in which the 10 m wind speed is equal to or lower than 4.0 m/s very likely caused the difference of ASCs.

Second, we conducted a cause analysis to identify the main factors leading to the increased number of ASCs in Shenzhen by analyzing the number of episodes selected or eliminated by each identification condition. As shown in Table 1, these identification condition can be classified

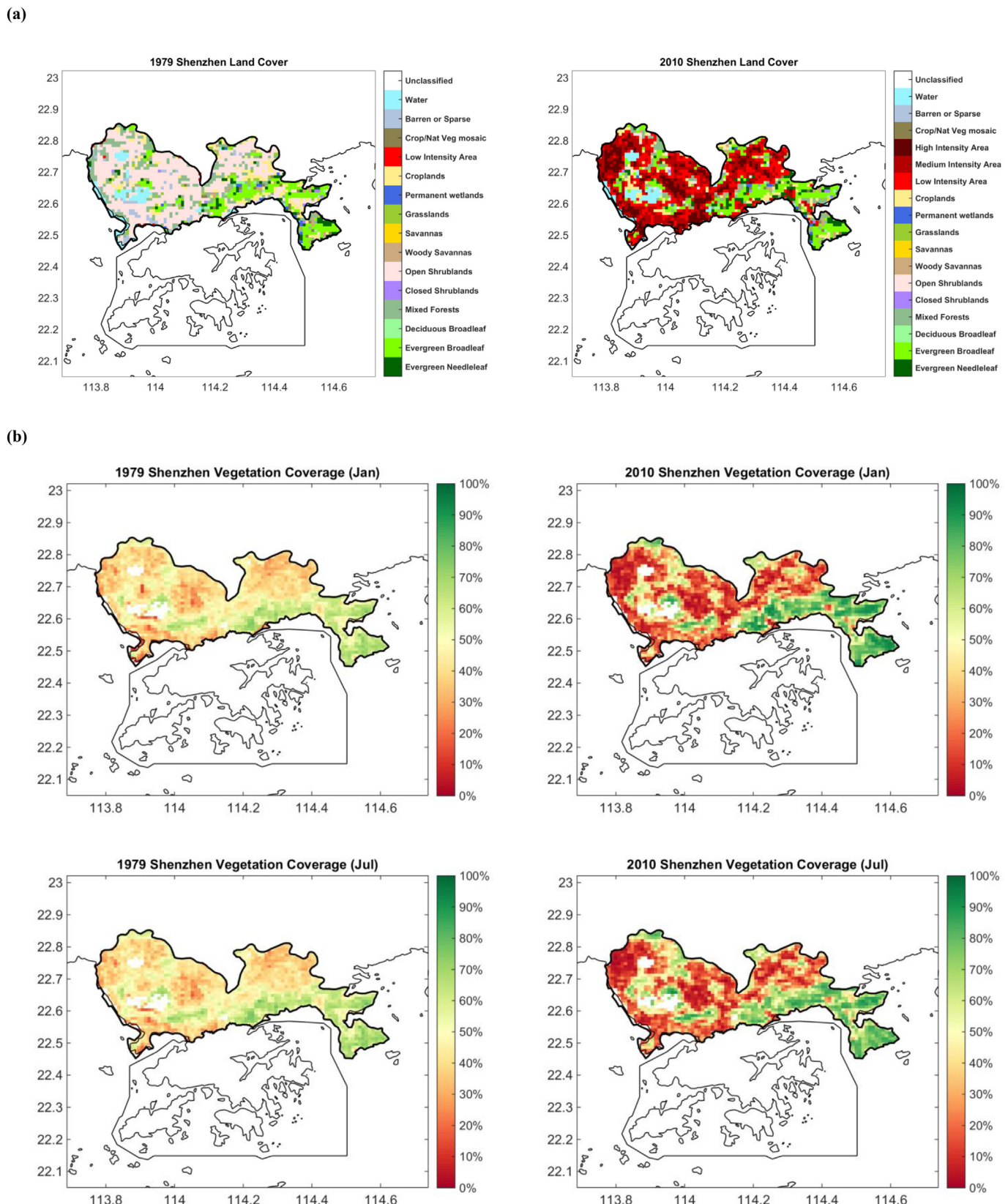
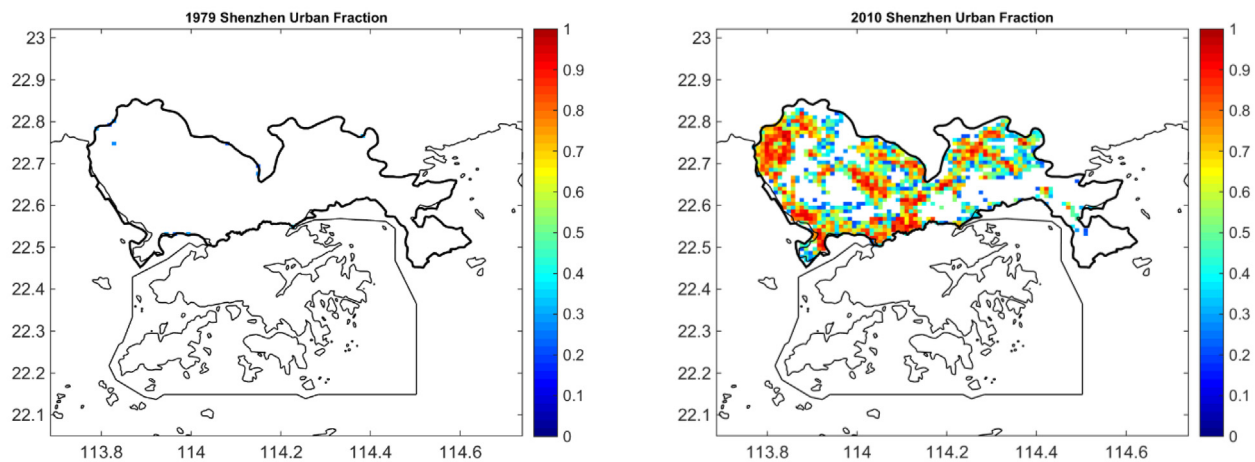


Fig. 2. Changes in land cover (a) and changes in monthly vegetation coverage in January (winter) and July (summer) in 1979 and 2010 (b). For vegetation coverage in other months, please refer to the Supplementary materials.

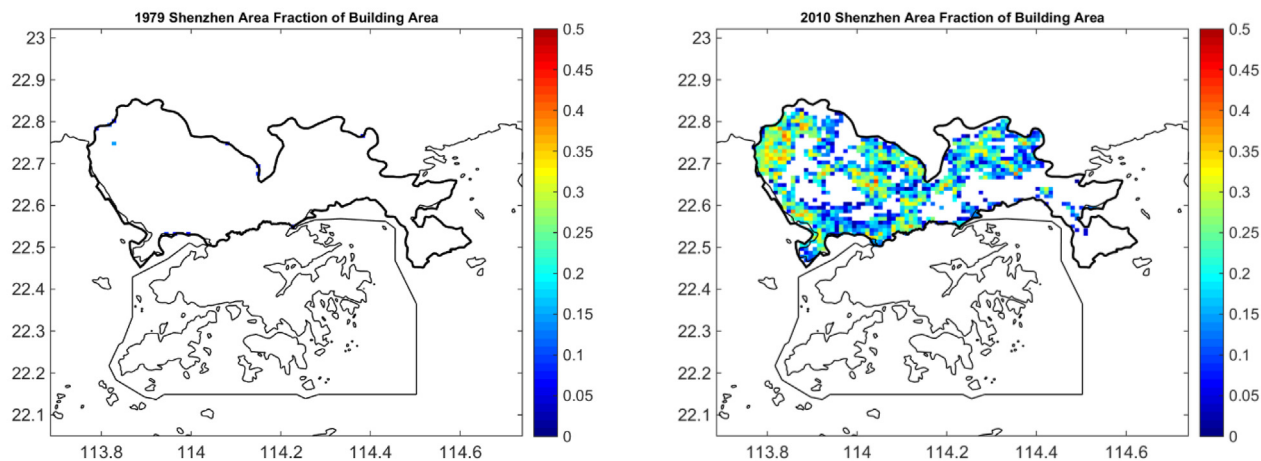
into two-condition sets (selection and elimination condition sets), the selection condition set for selecting air stagnation candidates from the 6-hourly grid meteorological episodes and the elimination condition

set for eliminating some 6-hourly grid meteorological episodes from the air stagnation candidates. The air stagnation candidates selected by using the selection conditions of S1, S2 and S3 increased by 17,352,

(a)



(b)



(c)

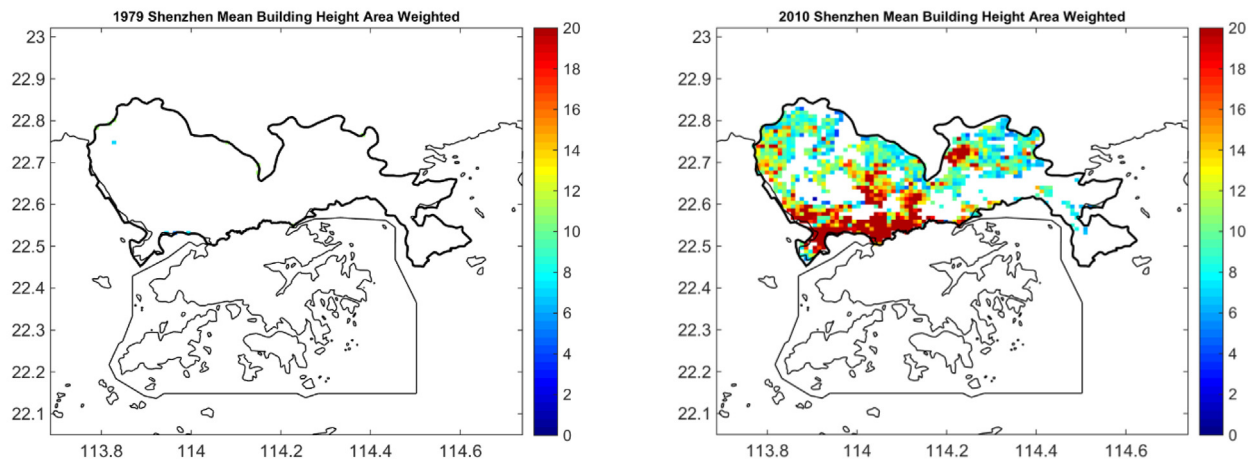
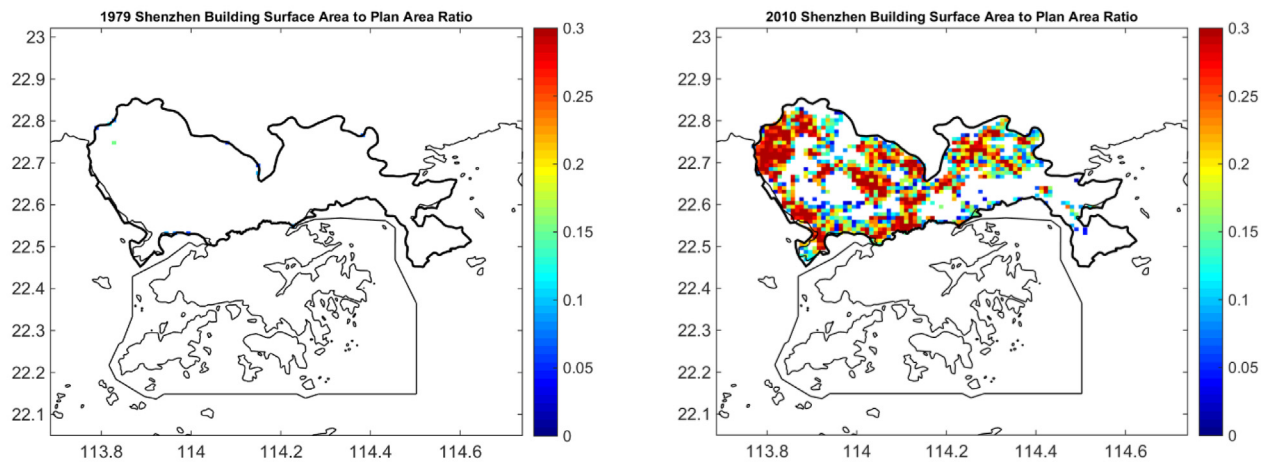
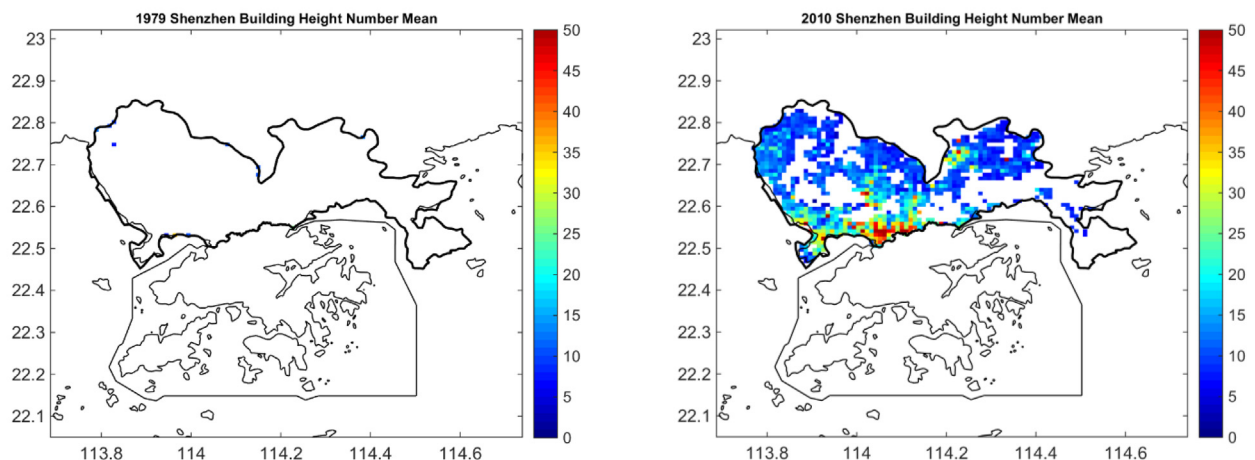


Fig. 3. Differences between 1979 and 2010 in urban morphology indicators in Shenzhen. Indicators include: (a) urban fraction, (b) area fraction of building area, (c) mean building height area weighted, (d) building surface area to plan area ratio, (e) building height number mean, (f) standard deviation of mean building height area weighted and (g) frontal area index.

(d)



(e)



(f)

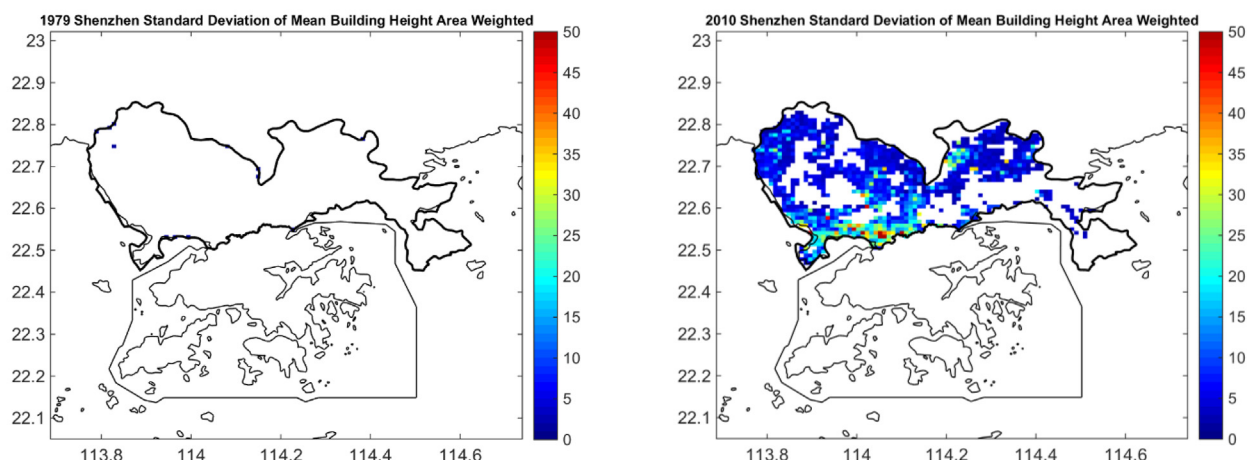
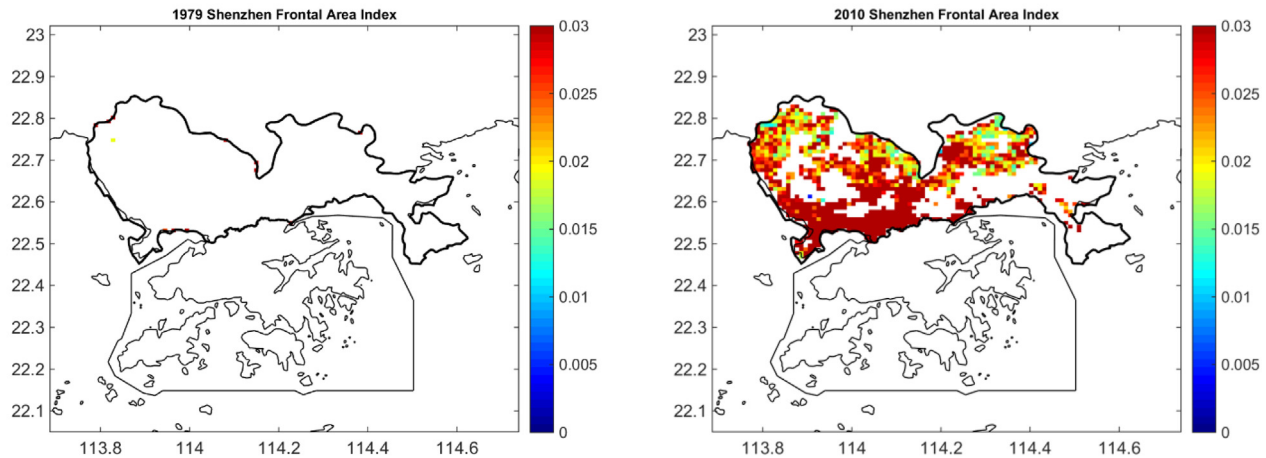


Fig. 3 (continued).

(g)

**Fig. 3 (continued).**

6798 and 3379 respectively in Case-2010 with respect to Case-1979, and accordingly air stagnation candidates totally increased by 27,529 in Case-2010. The number of eliminated candidates using elimination conditions of E4, E5 and E6 increased by 1615, 1021 and 3174 respectively in Case-2010 with respect to Case-1979, and accordingly eliminated candidates totally increased by 5810 in Case-2010. The percentages of the number of eliminated candidates to the number of total candidates are 45.9% in Case-2010 and 44.2% in Case-1979, which most probably implicates a slight increase of 1.7% in the number of grid meteorological episodes matching the elimination conditions in Case-2010. Although the annual number of air stagnation candidates matching the elimination conditions has a slight increase in Case-2010 with respect to Case-1979, it is far less than the increase in the annual number of the air stagnation candidates in Case-2010 with respect to Case-1979. Moreover, the numbers of the 6-hourly grid meteorological episodes in which the 10-m wind speed is equal to or lower than 4.0 m/s, the 10-m wind speed is higher than 4.0 m/s but equal to or lower than 4.4 m/s and a temperature inversion exists under the height of 850 mbar increased by 20,731, 12,169 and 14,007. Therefore, this analysis identifies the following main causes leading to an increase in the number of ASCs in Case-2010 with respect to Case-1979 (for the complete derivation process, please refer to Section S5 in Supplementary material):

- 1) The increase in the number of air stagnation candidates was caused by the increase in the number of meteorological episodes in which 10-m wind speed is equal to or lower than 4.4 m/s, especially the increase in the number of meteorological episodes in which 10-m wind speed is equal to or lower than 4.0 m/s.
- 2) The increase in the number of temperature inversion events enhanced the probability of the occurrence of air stagnation candidates having 10-m wind speed between 4.0 m/s and 4.4 m/s.

Third, only the difference in the number of the 6-hourly grid meteorological episodes in which 10-m wind speed is equal to or lower than 4.0 m/s has almost the same spatial distribution pattern as the one in Fig. 5. Therefore, this analysis identifies the reduction of the 10 m wind speed as the major cause of the increase of ASCs in 2010 (for the complete derivation process, please refer to Section S6 in Supplementary material).

Fourth, the spatial distribution pattern of the difference between Case-1979 and Case-2010 in the annual mean 10-m wind speed (Fig. 7a) is similar to that of the number of grid meteorological episodes in which 10-m wind speed is equal to or lower than 4.4 m/s (Fig. 7b). Moreover, the number of grid meteorological episodes in which the 10-m wind speed is equal to or lower than 4.4 m/s increases in the areas where the annual mean 10-m wind speed decreases; on the other hand, the number decreases in the areas where the speed increases. Therefore, there is an inverse proportional relationship between the change of annual mean 10-m wind speed and the difference in the number of grid meteorological episodes in which 10-m wind speed is equal to or lower than 4.4 m/s.

Therefore, the above analyses indicated the following main causes leading to the changes in ASCs:

- 1) The decrease in the 10-m wind speed in Case-2010 with respect to Case-1979 caused an increase in ASCs in Case-2010 with respect to Case-1979. Moreover, the spatial distribution pattern of the difference between two cases in the wind speed shaped the one of the difference of ASCs.
- 2) The increase in the number of grid temperature inversion enhanced the probability which the 6-hourly grid meteorological episodes become air stagnation cases.

5.2. Physical explanations of impact of urbanization on the 10-m wind speed

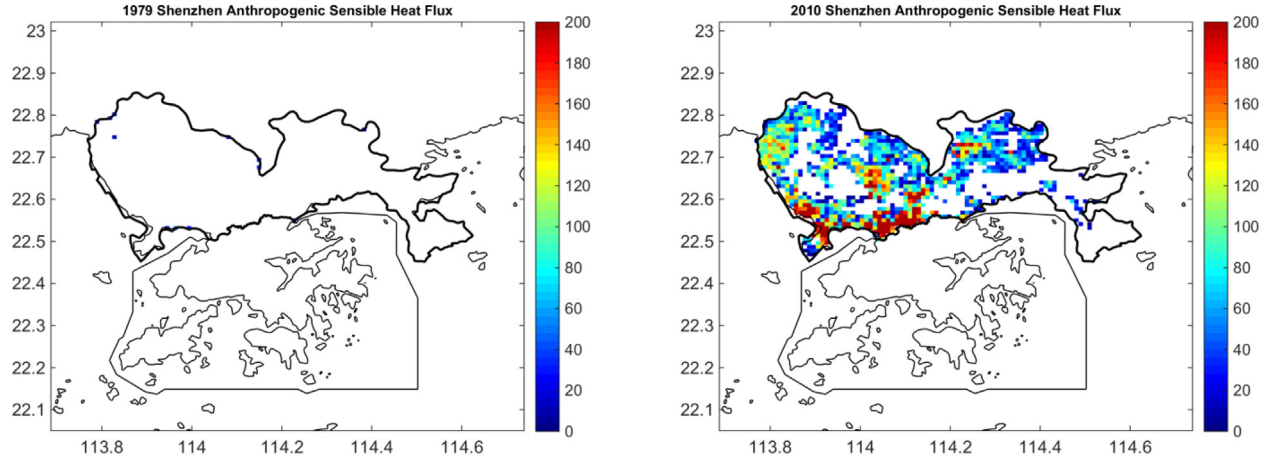
This subsection provides an explanation for the decrease in the 10-m wind speed after urbanization (Case-2010) and an explanation for the spatial distribution pattern of the difference between Case-2010 and Case-1979 in the 10-m wind speed.

First, the WRF/ARW/Noah LSM/SLUCM model calculates wind speed inside the PBL using the formula (Eq. (1)) based on the Monin-Obukhov similarity theory (Monin and Obukhov, 1954).

$$V = \frac{u_*}{k} \ln \frac{z-d}{Z_0} \quad (1)$$

where z is the height, V is the wind speed at the height of z , u_* is the friction velocity, k is the Von Karman constant (k is set to 0.4 in the model), d is the zero-plane displacement height, and Z_0 is the roughness length.

(a)



(b)

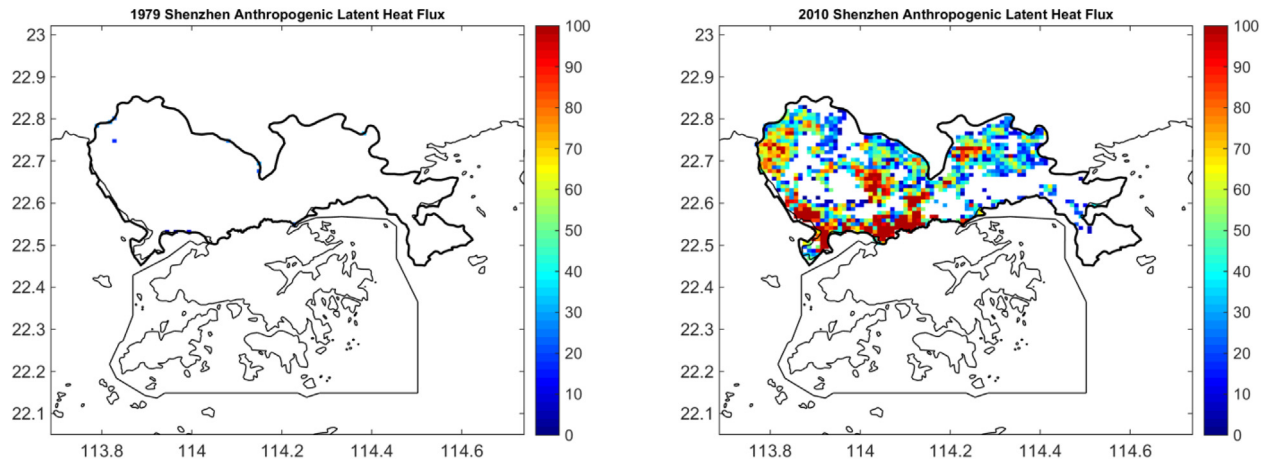


Fig. 4. Changes in the anthropogenic sensible heat flux (a) and anthropogenic latent heat flux (b) in Shenzhen in 1979 and 2010.

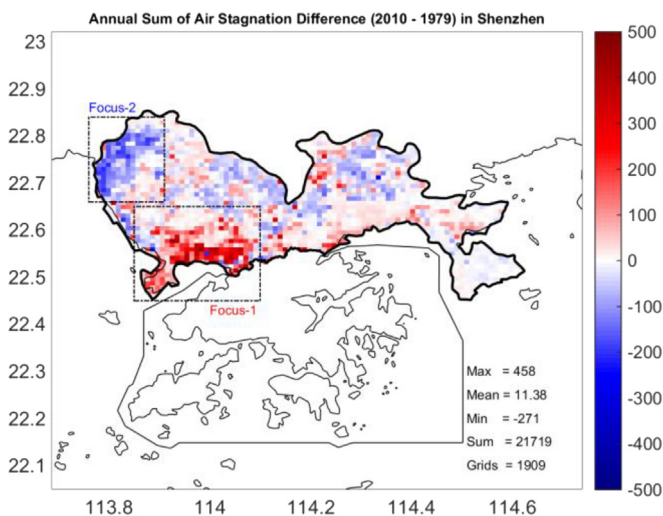


Fig. 5. The spatial distribution of the difference in the total annual number of ASCs between Case-1979 and Case-2010.

Moreover, the height of 10-m wind speed is set to the sum of the zero-plane displacement height and 10 m ($z = 10 + d$) in calculating the 10-m wind speed of a grid (Chen et al., 2011). Therefore, k was replaced with 0.4 and z replaced with $10 + d$ in Eq. (1) to calculate the 10-m wind speed of a grid (V_{10}) as

$$V_{10} \approx \frac{u_*}{0.4} \ln \frac{10}{Z_0} \quad (2)$$

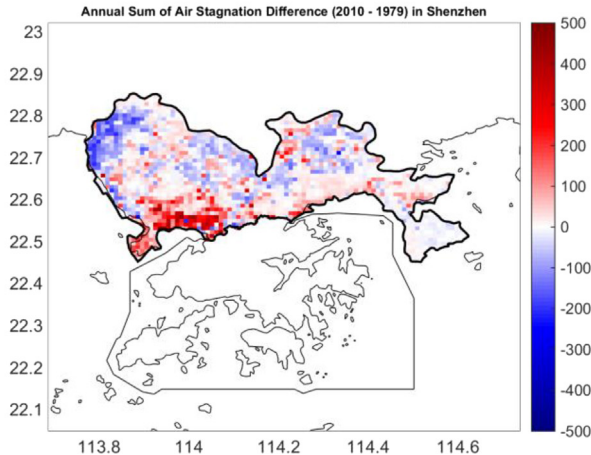
where V_{10} is 10-m wind speed of a grid, u_* is the friction velocity of this grid and Z_0 is the roughness length of this grid. Furthermore, the difference between Case-2010 and Case-1979 in the 10-m wind speed of a grid was calculated by Eq. (3).

$$\Delta v = V_{10,2010} - V_{10,1979} \quad (3)$$

where Δv is the difference between Case-2010 and Case-1979 in the 10-m wind speed of a grid, $V_{10,2010}$ is the 10-m wind speed of a grid in the Case-2010, and $V_{10,1979}$ is the 10-m wind speed of a grid in the Case-1979.

Second, among grids whose land cover is urban in Case-2010, most of the grids have a land cover category of open shrubland in Case-1979 (as shown in Fig. 2a). In the WRF ARW Noah LSM/SLUCM model, the roughness length of open shrubland grid is 0.03 (Chen et al.,

(a)



(b)

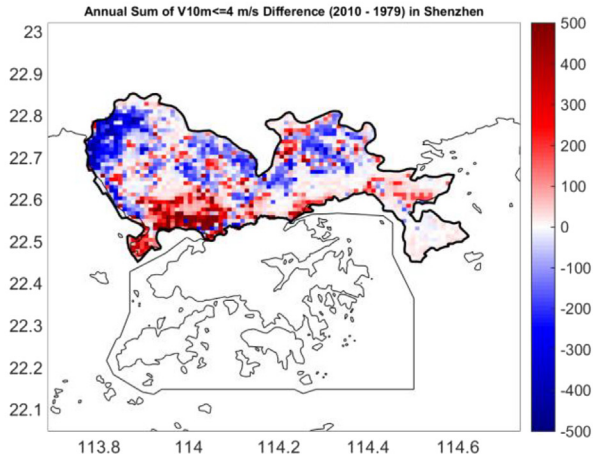


Fig. 6. Differences in the annual number of ASCs (a) and in the annual number of grid meteorological episodes in which 10-m wind speed is equal to or lower than 4.0 m/s (b).

2011). Therefore, Z_0 was replaced with 0.3 in Eq. (2) to calculate approximately the 10-m wind speed in these grids in Case-1979 as

$$V10_{1979} \approx 14.5u_{*1979} \quad (4)$$

where $V10_{1979}$ is the 10-m wind speed of these grids in the Case-1979 and u_{*1979} is the friction velocity of these grids in the Case-1979. Moreover, eighty percentage of these grids have friction velocity values between 0.3 and 0.4 (for more details, please refer to Section S7 of Supplementary material), and accordingly the friction velocity was set to 0.35 for the grids for further simplification of Eq. (4). Therefore, u_{*1979} was replaced with 0.35 in Eq. (4) to calculate the approximate 10-m wind speed of these grids as

$$V10_{1979} \approx 5.075 \quad (5)$$

where $V10_{1979}$ is the 10-m wind speed of these grids in the Case-1979.

Third, $V10_{2010}$ was replaced with $\frac{u_{*2010}}{0.4} \ln \frac{10}{Z0_{2010}}$ and $V10_{1979}$ was replaced with 5.075 in Eq. (3) for calculating the difference between Case-2010 and Case-1979 in the 10-m wind speed of a grid whose land cover category is urban in Case-2010 as

$$\Delta v \approx \frac{u_{*2010}}{0.4} \ln \frac{10}{Z0_{2010}} - 5.075 \quad (6)$$

Table 1
Selection and elimination conditions.

Conditions set	ID	Condition
Selection conditions	S1	Presence of a temperature inversion under the height of 850 mbar, and the 10-m wind speed is lower than 4.0 m/s.
	S2	Presence of a temperature inversion under the height of 850 mbar, and the 10-m wind speed is equal to or higher than 4.0 m/s but lower than 4.4 m/s.
	S3	Absence of a temperature inversion under the height of 850 mbar, and the 10-m wind speed is lower than 4.0 m/s.
Elimination conditions	E4	The grid precipitation is higher than 1 mm, and the 850-mbar wind speed is equal or lower than 13.0 m/s.
	E5	The grid precipitation is higher than 1 mm, and the 850-mbar wind speed is higher than 13.0 m/s.
	E6	The grid precipitation is equal to or lower than 1 mm, the 850-mbar wind speed is higher than 13.0 m/s, and absence of a temperature inversion under the height of 850 mbar.

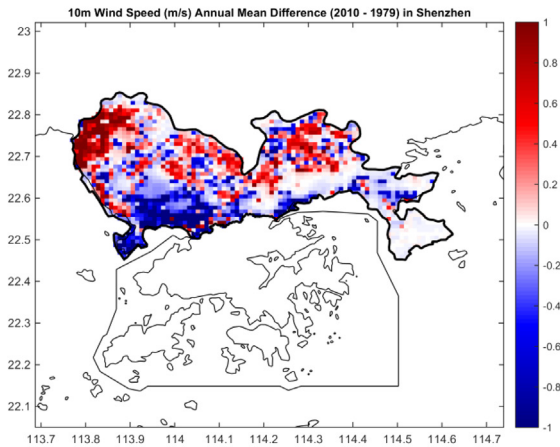
where Δv is the difference between Case-2010 and Case-1979 in the 10-m wind speed of a grid whose land cover category is urban in Case-2010, $Z0_{2010}$ is the roughness of this grid in the Case-2010, and u_{*2010} is the friction velocity of this grid in the Case-2010.

Fourth, Fig. 8, produced according to Eq. (6), shows the relationship between the difference in 10-m wind speed and the friction velocity at different roughness. As shown in Fig. 8, the difference between two cases in the 10-m wind speed is directly proportional to the friction velocity in Case-2010. For a given roughness, the difference increases with increasing friction velocity. In particular, the difference might possibly exceed 0 in case the roughness is small enough (e.g., the relation curve at the roughness of 0.25 m). However, it is evident that the slope of the relationship curve is inversely proportional to roughness. With an increase in roughness, the relationship curve would gradually become almost horizontal from upward sloping. This clarifies that the flexibility in the relationship between the difference and friction velocity would reduce to almost 0 from a positive value. The acceleration of increase in the relationship curves decreases to almost 0 with increasing roughness, i.e., if the roughness is long enough then it is possible that the difference is a negative value at almost the same level, independent from the friction velocity. For example, the acceleration of increase in the relationship curve decreases to almost 0 at the roughness of 10.0 m. These laws found in the relationships between 10-m wind speed, friction velocity, and roughness will be used in explanations for the change in the annual mean 10-m wind speed and the difference between Case-2010 and Case-1979 in the number of grid meteorological episodes in which 10-m wind speed is equal to or lower than 4.4 m/s.

Fifth, the friction velocity ranges between 0.21 and 0.98 and fluctuates slightly around the mean value of 0.43 (for more details, please refer to Section S8 of Supplementary material). On the other hand, the roughness ranges between 0.0 and 10.0 m, has a mean value of 0.6 m, and the roughness of 73% of the grids is over 0.1 m (for more details, please refer to Section S8 of Supplementary material). Taking these into consideration and using Eq. (6) to evaluate the difference between Case-2010 and Case-1979 in annual mean 10-m wind speed, it is not difficult to conclude that the annual mean 10-m wind speed of most grids in Case-2010 decreased. Therefore, according to the above laws, the increase of roughness caused the annual mean 10-m wind speed of most of the grids to decrease in Case-2010 and also caused an increase in the number of grid meteorological episodes in which 10-m wind speed is equal to or lower than 4.4 m/s in Case-2010.

Sixth, Fig. 9a shows that the values of friction velocity and roughness are higher in Focus-1 area. The roughness of most grids in Focus-1 area

(a)



(b)

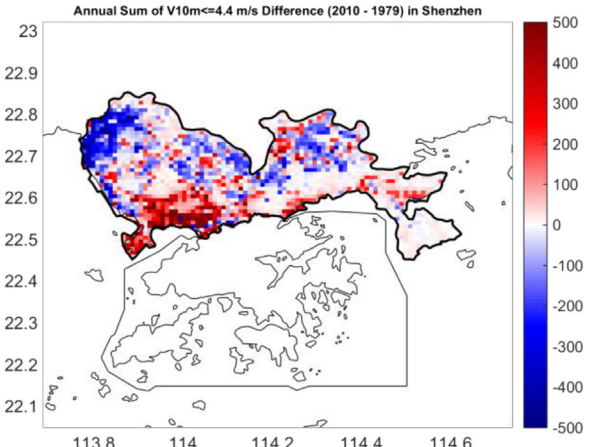


Fig. 7. Changes in the annual mean 10-m wind speed (a) and the number of meteorological episodes satisfying $V_{10m} \leq 4.4$ m/s (b) in Shenzhen.

is long enough to lessen the flexibility in the relationship curve, and accordingly, the value of the difference between Case-2010 and Case-1979 in 10-m wind speed of most grids in Focus-1 area is a negative value, although the grids have a higher value of friction velocity. In other words, the roughness of most grids in Focus-1 area largely increased in Case-2010 resulted in its annual mean 10-m wind speed decreased significantly. As for Focus-2 area, the roughness of most grids is small, but its friction velocity is sufficiently high. As a result, its 10-m wind speed increased in Case-2010 as compared to Case-1979. Therefore, the spatial variation patterns of roughness and friction velocity in Case-2010 cause the spatial variation of the differences between Case-2010 and Case-1979 in annual mean 10-m wind speed which resulted in the spatial variation of the difference between Case-2010 and Case-1979 in the number of grid meteorological episodes in which 10-m wind speed is equal to or lower than 4.4 m/s.

Seventh, the increase in urbanized land caused a decrease of albedo (Fig. 10a), which in turn caused an increase of surface sensible heat flux. Moreover, increase in urbanized land also caused an increase in sensible anthropogenic heat emission (Fig. 10b), which also caused an increase in surface sensible heat flux. Furthermore, the surface sensible heat

flux of most grids increased in Case-2010 (Fig. 10c), thereby making the atmospheric turbulence more vigorous in Case-2010. Therefore, the friction velocity of most grids increased in Case-2010 with respect to Case-1979.

Finally, explanations for the changes in 10-m wind speed can be summarized as follows:

- 1) The interaction between the roughness and the friction velocity determines the 10-m wind speed.
- 2) The urbanization in the city of Shenzhen in Case-2010 significantly increased the roughness of most grids. The significant increases in the roughness increased the number of grid meteorological episodes having a 10-m wind speed equal to or lower than 4.4 m/s.
- 3) Urbanization increased the anthropogenic heat and decreased the surface albedo excessively in Case-2010, which increased the surface sensible heat flux. Due to the increase in surface sensible heat flux, surface turbulences thrived leading to higher friction velocity in Case-2010 compared to that in Case-1979.
- 4) The decrease in roughness and the increase in friction velocity to appropriate values may increase the 10-m wind speed in Case-2010 with respect to Case-1979.
- 5) In the Focus-2 area, 10-m wind speed in most grids increased in Case-2010 due to the small increase in the roughness and friction velocity caused by the increase in surface sensible heat flux. Therefore, in Case-2010, there are a smaller number of grid meteorological episodes in which 10-m wind speed is equal to or lower than 4.4 m/s in Focus-2 area due to which the 10 m wind speed increase. On the other hand, although the friction velocity increased in Case-2010, the value of the roughness length was enough to make the relationship curve to lose its flexibility, which resulted in a significant decrease in the 10 m wind speed of most grids in Focus-1 area in Case-2010 with respect to Case-1979. As a result, in Case-2010, more grid meteorological episodes where 10 m wind speed is equal to or lower than 4.4 m/s in Focus-1 area were observed.

5.3. Physical explanations for the increase of temperature inversion episodes

This subsection provides an explanation for the increase in the number of temperature inversion episodes in Case-2010 with respect to Case-1979. The number of temperature inversion episodes of most land grids increased by 50 to 100 in Case-2010 (Fig. 11a). A temperature inversion is usually not caused by a single factor, but by a variety of

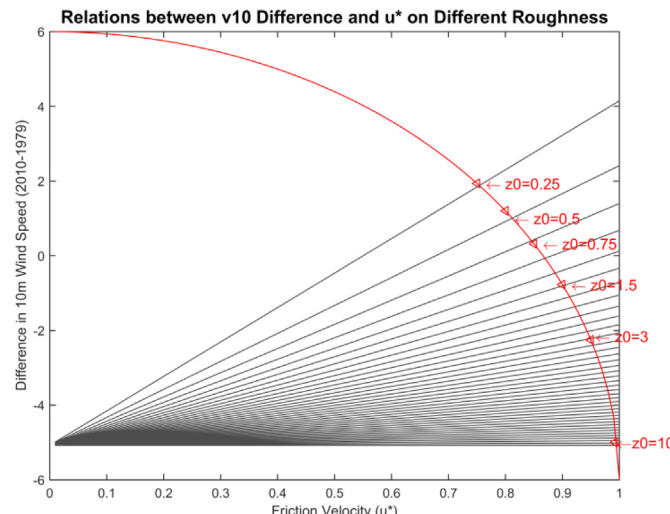
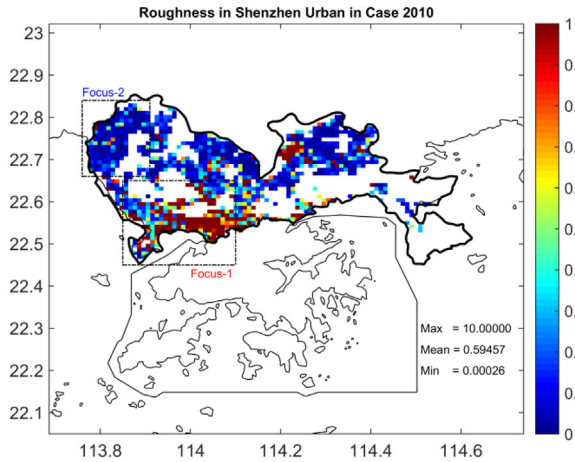


Fig. 8. Relationships between Δv and u^* for different z_0 .

(a)



(b)

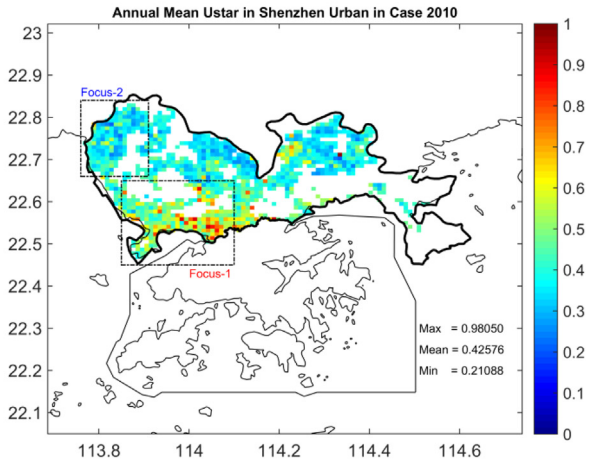
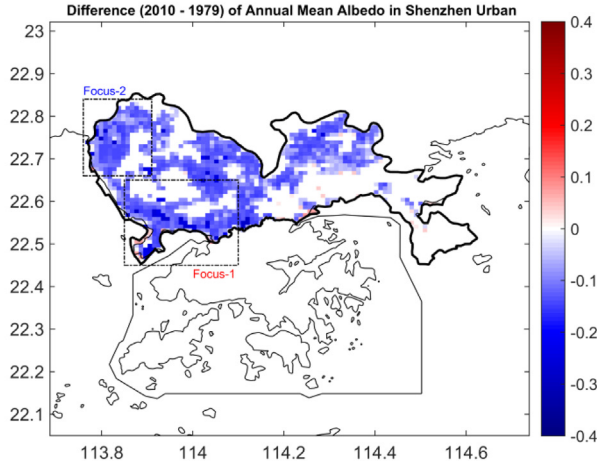


Fig. 9. The roughness (a) and annual mean friction velocity (b) in Shenzhen urban area in Case-2010.

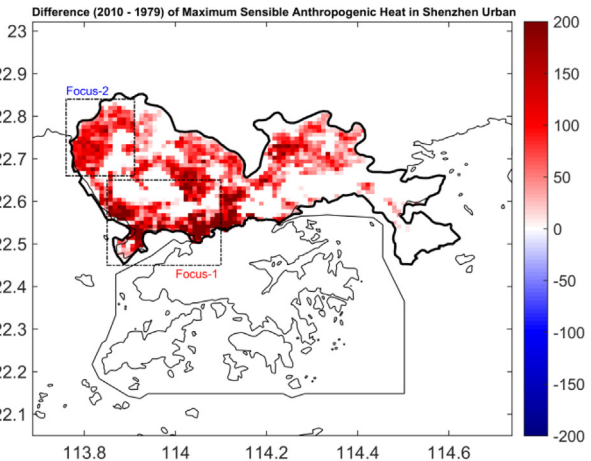
factors. These factors can be mainly classified into the following categories: Turbulence, Radiation, Air Subsidence, Frontal Grand and Air Advection.

The surface sensible heat flux of the Shenzhen in Case-2010 is much higher than that in Case-1079 (Fig. 11b). The surface sensible heat flux increased with the decrease in the surface albedo and increase in the

(a)



(b)



(c)

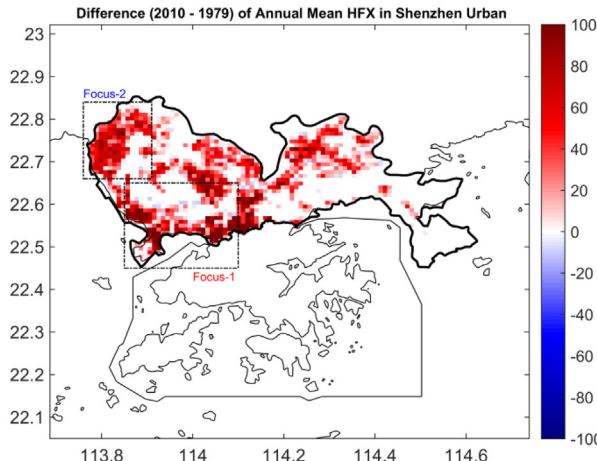


Fig. 10. Differences in annual mean albedo (a), maximum sensible anthropogenic heat (b) and annual mean surface sensible heat flux (c) between Case-2010 and Case-1979 in Shenzhen urban area.

sensible anthropogenic heat. Consequently, the increased surface sensible heat flux resulted in more vigorous atmospheric turbulences in Case-2010. In addition, the atmospheric temperature decreases with increased height in the turbulent mixing layer. However, the temperature inversion is created in the turbulence weakening layer which is a layer

between the lower layer (the turbulent mixing layer) and the upper layer in which the turbulent mixing does not occur. The increase in surface sensible heat flux enhances the atmospheric turbulence cooling effect on the top tier air of the turbulent mixing layer, and accordingly the temperature of top-tier air decreases. The upper layer atop of turbulent

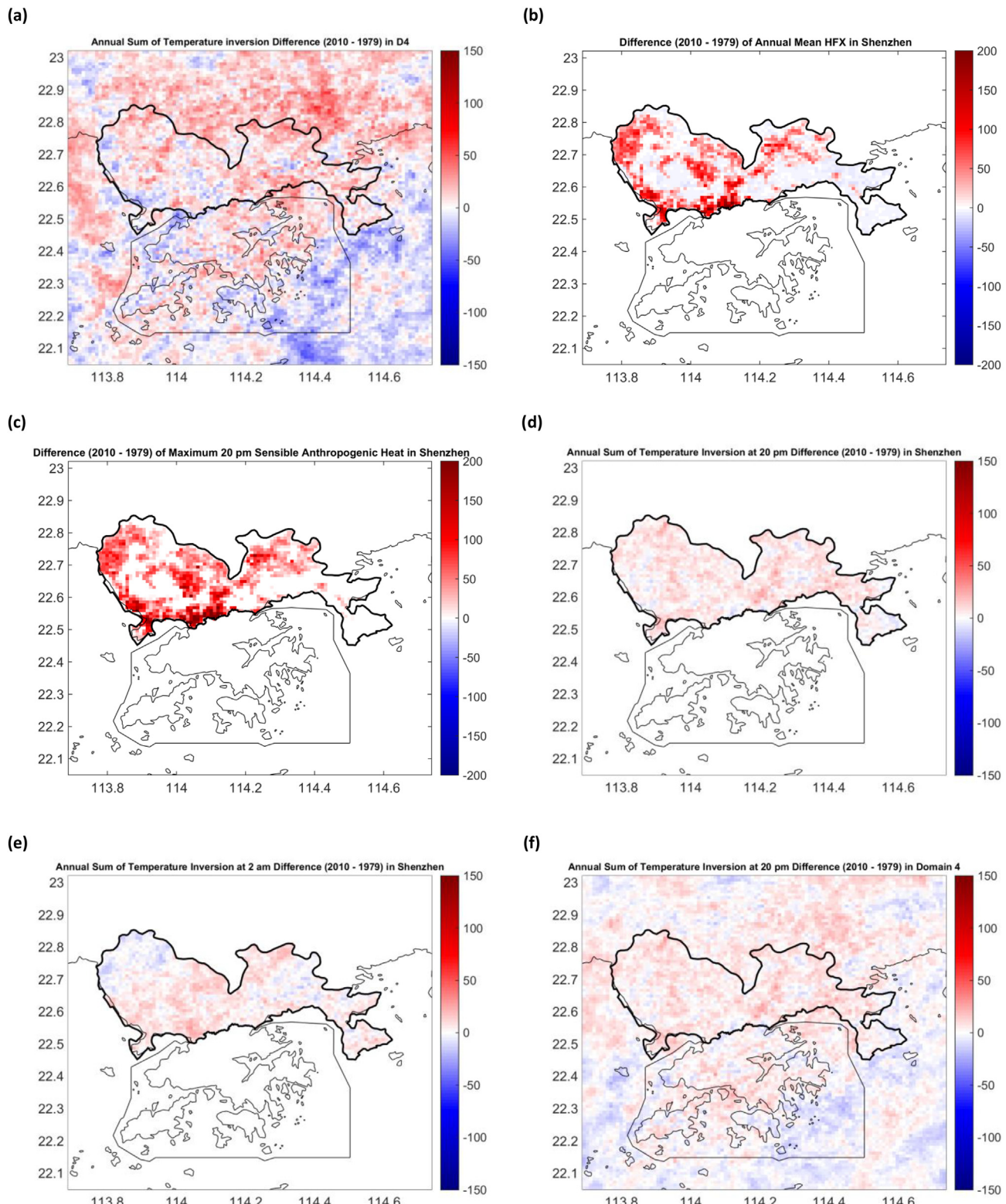


Fig. 11. Differences in the annual sum temperature inversion in domain 4 (a), annual mean surface sensible heat flux in Shenzhen (b), maximum sensible anthropogenic heat at 20:00 in Shenzhen (c), annual sum of temperature inversion at 20:00 in Shenzhen (d), annual sum of temperature inversion at 2:00 in Shenzhen (e), an annual sum of temperature inversion at 20:00 in domain 4 (f) and an annual sum of temperature inversion at 2:00 in domain 4 (g) between Case-2010 and Case-1979.

mixing layer keeps the original temperature while the temperature of top-tier air of the turbulent mixing layer decreases because the atmospheric turbulence does not influence this layer, and accordingly more temperature inversions are created in the turbulence weakening layer. This mechanism analysis also coincides with the results of Wan et al. (2017) research. The atmosphere under the height of 850 mbar includes the turbulence weakening layer and the upper layer without turbulent mixing. Therefore, more turbulence temperature inversion episodes were formed under the height of 850 mbar in Case-2010.

The urbanization of the Shenzhen area resulted in a decrease of the albedo from 1979 to 2010, which increased the surface temperature and in turn enhanced the radiation cooling effect at night. The sensible anthropogenic heat increased at 20:00 in the urban area (Fig. 11c), and accordingly, the surface atmospheric turbulences also thrived due to the increase in nighttime sensible anthropogenic heat in the urban area. It speeded up heat transfer vertically; thereby heating the upper air rapidly and causing more radiation temperature inversion episodes. Moreover, the radiation temperature inversion often occurs at night time. It is an evidence that the numbers of both 20:00 and 2:00 temperature inversion episodes (Fig. 11d and e) of most grids of Shenzhen, and especially those at 20:00, increased in Case-2010 in comparison to Case-1979. Therefore, more episodes of radiation temperature inversion occurred in Case-2010 with respect to that in Case-1979.

As shown in Fig. 11f and g, more temperature inversions were observed at 2:00 and especially at 20:00 in the north-western areas where non-urban land was still present in Case-2010. Therefore, as most of the land in Shenzhen area was already urbanized in Case-2010, more episodes of air advection temperature inversions were observed at night in non-urban areas (Fig. 2a).

To sum up, the increase in the number of temperature inversion events in Case-2010 can be explained as follows:

- 1) The urbanization in large areas of Shenzhen from 1979 to 2010 decreased the surface albedo and increased the sensible anthropogenic heat. As a result, the surface sensible heat increased from 1979 to 2010, which led to a more active atmospheric turbulence and more episodes of turbulent temperature inversion.
- 2) More episodes of radiation temperature inversion were observed in Case-2010 compared to Case-1979, because the decreased surface albedo enhanced the radiation cooling effect, while the increased sensible anthropogenic heat elevated this trend.
- 3) More episodes of advection temperature inversion were observed in the non-urban area in Case-2010 compared to Case-1979 due to the massive urbanization in its neighboured areas.

5.4. Impact of urbanization on ASC

Urbanization caused an increase in the annual number of ASCs, which replies to the research topic about the urbanization impact on air stagnation. Urbanization led to the increase in roughness, which results in a decrease in 10-m wind speed. The decrease in 10-m wind speed resulted in an increase of the number of grid meteorological episodes reaching the threshold for lower atmospheric horizontal movement and therefore becoming air stagnation candidates. Moreover, a decrease in albedo and increase in sensible anthropogenic heat emission caused the increase of surface sensible heat flux, thereby triggering more temperature inversion episodes. This also produced more air stagnation candidates. Furthermore, the number of meteorological episodes reaching the eliminating thresholds (convective and upper atmospheric movement) increased slightly. On the other hand, the annual number of air stagnation candidates increased rapidly. Therefore, the annual number of ASCs increased significantly after urbanization. To sum up, urbanization caused a reduction in surface wind speed to make the air stagnation more severe, and resulted in an increase in temperature inversion episodes to enhance the aggravation slightly, and accordingly, the number of ASCs increases significantly after urbanization.

Our results are also in agreement with previous researches. The studies of Elliott et al. (2004) and Jacobson et al. (2015), for instance, revealed the connection between the increase in urbanization and the decrease in wind speed, in good agreement with our results. The increase in the annual number of ASCs has also been observed in other fast-urbanizing cities such as Beijing (Jacobson et al., 2015; Huang et al., 2017).

Our research revealed the physical mechanism of the impacts of the changes in land cover, vegetation coverage, urban morphology and anthropogenic heat fluxes on air stagnation. However, besides these changes caused by urbanization, other factors also affect air stagnation. For example, Jacobson and Kaufman (2006) revealed that the increasing emission of anthropogenic aerosol particle and precursor gases reduces surface wind speed. The reduction in surface wind speed increases the number of ASCs. The increase in the emission of anthropogenic aerosol and precursor gases are also mainly due to the massive urbanization since urbanization dramatically increases local population and non-agricultural activities (Jacobson and Kaufman, 2006). Therefore, the increase in the emission of anthropogenic aerosol and precursor gases during urbanization also make air stagnation more severe.

The stricter criterion for identifying temperature inversion episodes with respect to atmospheric stable ones resulted accordingly in a reduced number of temperature inversion episodes. Indeed, although the air convective movement seldom occurs during an atmospheric stability episode, the pollutants can still diffuse quickly if the surface wind speed is large enough, and accordingly it became a common practice in the air stagnation researches to use temperature inversion as the criterion for increasing 10% of the atmospheric horizontal movement threshold (Korshover and Angell, 1982, 1987; Wang and Angell, 1999; Leung and Gustafson, 2005; Horton and Diffenbaugh, 2012; Horton et al., 2014). Moreover, we also conducted an uncertainty examination (Please refer to Section S4 of Supplementary material) on alternating the criterion based on the lapse rate changes ($-0.98, -0.65, -0.40$) while no significant changes in the result were found. For more details, please refer to Section S9 of Supplementary material.

6. Conclusions

Taking Shenzhen, China as a compelling case study, we first carefully defined the identifying criteria for ASCs based on the physical mechanism of air stagnation explained in existing literature. Using the proposed criteria, we then identified and evaluated ASCs in Shenzhen with high spatial-temporal resolution. The identification was enabled by high-resolution urban climate simulation using the WRF/Noah LSM/SLUCM model with an improved urban land surface dataset that integrated detailed urbanization-induced spatial-temporal changes in land cover, vegetation coverage, urban morphology, and anthropogenic heat fluxes. We observed a significant increase in the frequency of ASCs after thirty years' rapid urbanization in Shenzhen. The proposed methodology for evaluating urban air stagnation at fine spatial-temporal scales can be applied in many other cities. Our discussions on the impact of urbanization on ASCs help derive policies that control air pollution with regulated urban changes.

With a sophisticated cause analysis, we were able to conclude that urbanization has a regulating mechanism on air stagnation (Fig. 12). Urbanization significantly alters the land surface process by increasing the roughness, decreasing the albedo of land surface, and releasing more sensible anthropogenic heat into the near-surface atmosphere. During urbanization, the change in population affects the emission of sensible anthropogenic heat, changes in land cover and vegetation coverage affect the albedo, and the change in urban morphology affects the roughness. Moreover, the change in albedo, in turn affects the surface sensible heat flux and the number of temperature inversion episodes. The change in sensible anthropogenic heat also affects surface sensible heat flux. The change in surface sensible heat flux causes the atmospheric turbulences to thrive. The change in the atmospheric turbulence

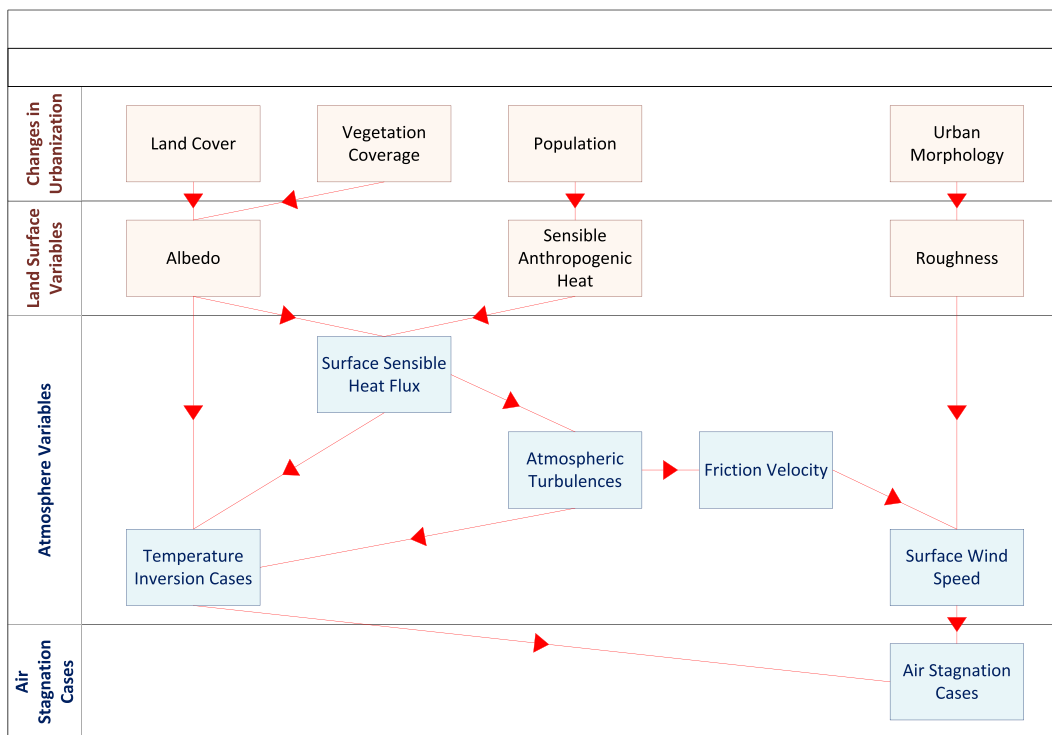


Fig. 12. The regulating mechanism leading to the changes in the number of ASCs. Red arrows indicate the directions of the impacts.

affects the friction velocity. The changes in roughness and the friction velocity affect the surface wind speed. Furthermore, the number of temperature inversion cases is affected by the changes in surface sensible heat flux and atmospheric turbulence. Finally, the changes in temperature inversion and surface wind speed make an impact on air stagnation.

Code availability

Information on the availability of source codes used in this study is listed below.

Source codes	Availability
WRF Model 3.7.1	These source codes are publicly available at http://www2.mmm.ucar.edu/wrf/users/download/get_source.html
WRF Pre-Processing System (WPS) 3.7.1	These source codes are publicly available at http://www2.mmm.ucar.edu/wrf/users/download/get_source.html
namelist.wps	These source codes are available upon request from the corresponding author.
namelist.input	These source codes are available upon request from the corresponding author.
Changes in the programs of WRF for inputting the 2D anthropogenic sensible and latent heat data	These source codes are available upon request from the corresponding author.
geo_data_refinement processing package	These source codes are available upon request from the corresponding author.
wrf_input_refinement processing package	These source codes are available upon request from the corresponding author.

Data availability

Information on the availability of data used in this paper is tabulated below.

Data	Availability
2010 NCEP FNL (Final)	This dataset is publically available at https://doi.org/10.1016/j.scitenv.2019.01.232 .

(continued)

Data	Availability
Operational Global Analysis Dataset	ucar.edu/datasets/ds083.2/
Completed Dataset of WRF Preprocessing System (WPS) Geographical Input Data	This dataset is publically available at http://www2.mmm.ucar.edu/wrf/users/download/get_sources_wps_geog.html
PRD Urban Land Surface Dataset	This dataset is available upon request from the corresponding author.
Simulation Output Dataset	

Competing interests

The authors declare that they have no conflict of interest.

Acknowledgements

This study was supported by National Key R&D Program of China (2017YFB0503605), which is gratefully acknowledged.

Appendix A. Supplementary data

Supplementary data to this article can be found online at <https://doi.org/10.1016/j.scitenv.2019.01.232>.

References

- Borsos, E., Makra, L., Béczki, R., Vitányi, B., Szentpéteri, M., 2003. Anthropogenic air pollution in the ancient times. *Acta Climatologica et Chorologica* 36 (37), 5–15.
- Chang, M., Fan, S.F., Wang, X.M., 2014. Impact of refined land-cover data on WRF performance over the Pearl River Delta region, China. *Acta Sci. Circumst.* 34 (8), 1922–1933.
- Chen, F., Kusaka, H., Bornstein, R., Ching, J., Grimmond, C.S.B., Grossman-Clarke, Thomas Loridan, Manning, Kevin W., Martilli, Alberto, Miao, Shiguang, Sailor, David, Salamanca, Francisco P., Taha, Haider, Tewari, Mukul, Wang, Xuemei, Wyszogrodzki, Andrzej A., Zhang, C., 2011. The integrated WRF/urban modelling system: development, evaluation, and applications to urban environmental problems. *Int. J. Climatol.* 31 (2), 273–288.

- Costa, S., Ferreira, J., Silveira, C., Costa, C., Lopes, D., Relvas, H., ... Paulo Teixeira, J., 2014. Integrating health on air quality assessment—review report on health risks of two major European outdoor air pollutants: PM and NO₂. *J. Toxicol. Environ. Health B* 17 (6), 307–340.
- Delfino, R.J., Staimer, N., Tjoa, T., Gillen, D., Kleinman, M.T., Sioutas, C., Cooper, D., 2008. Personal and ambient air pollution exposures and lung function decrements in children with asthma. *Environ. Health Perspect.* 116 (4), 550.
- Edussuriya, P., Chan, A., Malvin, A., 2014. Urban morphology and air quality in dense residential environments: correlations between morphological parameters and air pollution at street-level. *J. Eng. Technol.* 9 (1), 64–80.
- EEA, 2012. Air quality in Europe 2012 report. Copenhagen, Denmark. Retrieved November 10, 2016 from. <https://www.eea.europa.eu/publications/air-quality-in-europe-2012>.
- Elliott, D., Schwartz, M., Scott, G., 2004. Wind resource base. Encyclopedia of Energy vol. 6. Elsevier, New York, pp. 465–479.
- Fletcher, R.D., 1949. The Donora smog disaster—a problem in atmospheric pollution. *Weatherwise* 2 (3), 56–60.
- Halonen, J.I., Lanki, T., Yli-Tuomi, T., Kulmala, M., Tiittanen, P., Pekkanen, J., 2008. Urban air pollution and asthma and COPD hospital emergency room visits. *Thorax* 63 (7), 635–641.
- Havlíček, F., Morcinek, M., 2016. Waste and pollution in the ancient Roman empire. *J. Landsc. Ecol.* 9 (3), 33–49.
- He, K., Huo, H., Zhang, Q., 2002. Urban air pollution in China: current status, characteristics, and progress. *Annu. Rev. Energy Environ.* 27 (1), 397–431.
- Hewson, E.W., 1951. Atmospheric pollution. Compendium of Meteorology. American Meteorological Society, pp. 1139–1157.
- Horton, D.E., Difffenbaugh, N.S., 2012. Response of air stagnation frequency to anthropogenically enhanced radiative forcing. *Environ. Res. Lett.* 7 (4), 044034.
- Horton, D.E., Skinner, C.B., Singh, D., Difffenbaugh, N.S., 2014. Occurrence and persistence of future atmospheric stagnation events. *Nat. Clim. Chang.* 4 (8), 698–703.
- Huang, D., Xu, J., Zhang, S., 2012. Valuing the health risks of particulate air pollution in the Pearl River Delta, China. *Environ. Sci. Pol.* 15 (1), 38–47.
- Huang, Q., Cai, X., Song, Y., Zhu, T., 2017. Air stagnation in China (1985–2014): climatological mean features and trends. *Atmos. Chem. Phys.* 17 (12), 7793–7805.
- Jacob, D.J., Winner, D.A., 2009. Effect of climate change on air quality. *Atmos. Environ.* 43 (1), 51–63.
- Jacobson, M.Z., Kaufman, Y.J., 2006. Wind reduction by aerosol particles. *Geophys. Res. Lett.* 33 (24).
- Jacobson, M.Z., Nghiem, S.V., Sorichetta, A., Whitney, N., 2015. Ring of impact from the mega-urbanization of Beijing between 2000 and 2009. *J. Geophys. Res. Atmos.* 120 (12), 5740–5756.
- Korshover, J., 1976. Climatology of Stagnating Anticyclones East of the Rocky Mountains, 1936–1975. US Department of Health, Education, and Welfare, Division of Engineering Services.
- Korshover, J., Angell, J.K., 1982. A review of air-stagnation cases in the eastern United States during 1981—annual summary. *Mon. Weather Rev.* 110 (10), 1515–1518.
- Korshover, J., Angell, J.K., 1987. Air stagnation cases in the eastern United States during 1985. *Mon. Weather Rev.* 115 (1), 336–341.
- Leung, L.R., Gustafson, W.I., 2005. Potential regional climate change and implications to US air quality. *Geophys. Res. Lett.* 32 (16).
- Li, Z.Q., Zhou, Y.L., Wan, B.C., Huang, B., Liu, B., Chung, H.P., 2019d. Model evaluation of high-resolution urban climate simulations: using WRF ARW/LSM/SLUCM model as a case study. *Geosci. Model Dev. Discuss.* <https://doi.org/10.5194/gmd-2018-220>.
- Mar, T.F., Larson, T.V., Stier, R.A., Claiborn, C., Koenig, J.Q., 2004. An analysis of the association between respiratory symptoms in subjects with asthma and daily air pollution in Spokane, Washington. *Inhal. Toxicol.* 16 (13), 809–815.
- Matus, K., Nam, K.M., Selin, N.E., Lamsal, L.N., Reilly, J.M., Paltev, S., 2012. Health damages from air pollution in China. *Glob. Environ. Chang.* 22 (1), 55–66.
- Mayer, H., 1999. Air pollution in cities. *Atmospheric Environment.* 33 (24–25), 4029–4037.
- Monin, A.S., Obukhov, A.M.F., 1954. Basic associations of turbulent mixing in the surface layer of the atmosphere. *Contrib. Geophys. Inst. Acad. Sci. USSR* 151 (163), e187.
- Ng, E., Yuan, C., Chen, L., Ren, C., Fung, J.C., 2011. Improving the wind environment in high-density cities by understanding urban morphology and surface roughness: a study in Hong Kong. *Landsc. Urban Plan.* 101 (1), 59–74.
- Perkins, S.E., Pitman, A.J., Holbrook, N.J., McAneney, J., 2007. Evaluation of the AR4 climate models' simulated daily maximum temperature, minimum temperature, and precipitation over Australia using probability density functions. *J. Clim.* 20 (17), 4356–4376.
- Sarzynski, A., 2012. Bigger is not always better: a comparative analysis of cities and their air pollution impact. *Urban Stud.* 49 (14), 3121–3138.
- Statistics Bureau of Shenzhen Municipality, 2013. Shenzhen Annual Statistical Year Book 2012. Available at. <http://www.sztj.gov.cn/nj2012/start2012.htm>, Accessed date: 4 March 2015.
- Wan, B., Gao, Z., Chen, F., Lu, C., 2017. Impact of Tibetan Plateau surface heating on persistent extreme precipitation events in southeastern China. *Mon. Weather Rev.* 145 (9), 3485–3505.
- Wang, J.X., Angell, J.K., 1999. Air stagnation climatology for the United States. NOAA/Air Resource Laboratory ATLAS (1).
- Wang, W., Bruyere, C., Duda, M., Dudhia, J., Gill, D., Lin, H.C., ... Mandel, J., 2015. ARW version 3 modeling system user's guide July 2015. Retrieved September, 9, 2015, from. Mesoscale & Microscale Meteorology Division, National Center for Atmospheric Research http://www2.mmm.ucar.edu/wrf/users/docs/user_guide_V3/ARWUsersGuideV3.pdf.
- Willett, H.D., 1949. Some meteorological aspects of air pollution. *Trans. Conf. on Industrial Wastes, Ind. Hyg. Found., Amer. Trans. Bull.* (No. 13).
- World Health Organization, 2006. Air Quality Guidelines: Global Update 2005: Particulate Matter, Ozone, Nitrogen Dioxide, and Sulfur Dioxide. World Health Organization.
- Yim, S.H., Fung, J.C.H., Lau, A.K.H., Kot, S.C., 2009. Air ventilation impacts of the “wall effect” resulting from the alignment of high-rise buildings. *Atmos. Environ.* 43 (32), 4982–4994.
- Yuan, C., Ng, E., Norford, L.K., 2014. Improving air quality in high-density cities by understanding the relationship between air pollutant dispersion and urban morphologies. *Build. Environ.* 71, 245–258.
- Zhou, L., Dickinson, R.E., Tian, Y., Fang, J., Li, Q., Kaufmann, R.K., ... Myneni, R.B., 2004. Evidence for a significant urbanization effect on climate in China. *Proc. Natl. Acad. Sci. U. S. A.* 101 (26), 9540–9544.